doi:10.1093/brain/aww334

BRAIN
A JOURNAL OF NEUROLOGY

Relationships between flortaucipir PET tau binding and amyloid burden, clinical diagnosis, age and cognition

Michael J. Pontecorvo,[1] Michael D. Devous Sr,[1] Michael Navitsky,[1] Ming Lu,[1] Stephen Salloway,[2] Frederick W. Schaerf,[3] Danna Jennings,[4] Anupa K. Arora,[1] Anne McGeehan,[1] Nathaniel C. Lim,[1] Hui Xiong,[1] Abhinay D. Joshi,[1] Andrew Siderowf[1] and Mark A. Mintun[1] for the ^{18}F-AV-1451-A05 investigators

The advent of tau-targeted positron emission tomography tracers such as flortaucipir (^{18}F-AV-1451, also known as ^{18}F-T807) have made it possible to investigate the sequence of development of tau and amyloid-β in relationship to age, and to the development of cognitive impairment due to Alzheimer's disease. In this study, flortaucipir tau and florbetapir amyloid positron emission tomography were obtained for 217 subjects including 16 young and 58 older cognitively normal subjects, 95 subjects with mild cognitive impairment (Mini-Mental State Examination 24–30) and 48 subjects with clinically-defined possible or probable Alzheimer's disease (Mini-Mental State Examination >10). Images were evaluated visually and quantitatively by regional and voxel-based cortical to cerebellar standard uptake value ratios. For amyloid positron emission tomography positive (Aβ+) subjects, flortaucipir neocortical standard uptake value ratio was significantly higher with more advanced clinical stage (Alzheimer's disease > mild cognitive impairment > older cognitively normal) and was significantly elevated for Aβ+ mild cognitive impairment and Alzheimer's disease subjects relative to the respective Aβ− subjects. In contrast, florbetapir Aβ− older cognitively normal subjects showed an increase in flortaucipir standard uptake value ratios in mesial temporal lobe regions (amygdala, hippocampus/choroid plexus region of interest) compared to younger cognitively normal subjects, but no increased standard uptake value ratios in neocortical regions. Analysis of covariance with planned contrasts showed no differences in regional or composite posterior neocortical flortaucipir standard uptake value ratio as a function of diagnostic group among Aβ− older cognitively normal or clinically diagnosed Alzheimer's disease or mild cognitive impairment subjects. The pattern of flortaucipir distribution among Aβ+ subjects was reminiscent of the cross-sectional distribution of tau reported in post-mortem pathology studies, in that the most commonly affected regions were the inferior and lateral temporal lobes, the same regions where the first signs of increased retention appeared in Aβ+ cognitively normal subjects. However, there was large variability in extent/density of flortaucipir tau binding among Aβ+ subjects. Although high neocortical flortaucipir retention was consistently associated with an Aβ+ florbetapir positron emission tomography scan, not all Aβ+ subjects had elevated flortaucipir standard uptake value ratios. Finally, within the Aβ+ group, increasing levels of flortaucipir tau binding were associated with increased cognitive impairment, as assessed by Mini-Mental State Examination and Alzheimer's Disease Assessment Scale. These results suggest development of tau beyond the mesial temporal lobe is associated with, and may be dependent on, amyloid accumulation. Further, the results are consistent with the hypothesis that cortical tau is associated with cognitive impairment.

1 Avid Radiopharmaceuticals, Philadelphia, PA 19104, USA
2 Butler Hospital, Providence, RI, 02906, USA
3 Neuropsychiatric Research Center of Southwest Florida, Fort Myers, FL 33912, USA
4 Molecular Neuroimaging Inc., New Haven CT 06510, USA

Received July 20, 2016. Revised October 13, 2016. Accepted November 03, 2016.

Correspondence to: Michal Pontecorvo,
Avid Radiopharmaceuticals, Inc.,
3711 Market St. Philadelphia,
PA 19104, USA
E-mail: pontecorvo@avidrp.com

Keywords: tau; ^{18}F-AV-1451; flortaucipir; florbetapir; PET

Abbreviations: Aβ = amyloid-β; ADAS = Alzheimer's Disease Assessment Scale; MCI = mild cognitive impairment; MMSE = Mini-Mental State Examination; OCN = older cognitively normal; SUVr = standard uptake value ratio; YCN = young cognitively normal

Introduction

Pathological accumulation of hyperphosphorylated microtubule-associated tau protein (MAPT, tau) in neurons and glia underlies a wide range of neurodegenerative disorders. Alzheimer's disease is the most common tauopathy, affecting ~35 million people worldwide (Querfurth *et al.*, 2010). The Alzheimer's disease pathology is characterized by amyloid plaques composed largely of aggregated amyloid-β (Aβ) 1–42 fragments (Kidd *et al.*, 1963; Masters *et al.*, 1985) and tau-containing neurofibrillary tangles (Goedert *et al.*, 1992). Both amyloid plaques and neurofibrillary tangles are required to establish a neuropathologic diagnosis of Alzheimer's disease (Hyman *et al.*, 2012).

In animal models, the introduction of misfolded tau can alter neuronal excitability and synaptic plasticity *in vitro* and can induce, in living animals, behavioural deficits that vary with the placement of the abnormal tau seed (Pooler *et al.*, 2014; Stancu *et al.*, 2014). Correlative studies in post-mortem human tissue indicate that progressive tau-based neurofibrillary pathology is associated with the progressive clinical manifestations of Alzheimer's disease. While older subjects with no impairment can have neurofibrillary tangles in the entorhinal cortex and adjacent hippocampus (Bouras *et al.*, 1994), widespread neocortical tau deposition is only observed in subjects with significant cognitive impairment (Tomlinson *et al.*, 1970). Pathological series have shown that Braak Stage (Braak and Braak, 1991; Braak *et al.*, 2006), representing extent of tau pathology, correlates with cognitive status (Riley *et al.*, 2002) as does the density of neurofibrillary pathology assessed in various neocortical regions (Nelson *et al.*, 2007).

Because of its central role in Alzheimer's disease and other neurodegenerative disorders, the tau protein has emerged as an attractive therapeutic target. It has been argued that anti-tau therapeutics may be more efficacious than anti-amyloid approaches because tau is more closely associated with cell death in Alzheimer's disease (Giacobini *et al.*, 2013). Anti-tau therapeutic approaches have included attempts to restore the normal function of the tau protein by inhibition of tau phosphorylation (Del Ser *et al.*, 2013) and tau aggregation (Anand *et al.*, 2014). Other therapeutic strategies have focused on reducing accumulation or spread of tau aggregates (Holtzman *et al.*, 2016). Recently, infusion of an anti-tau antibody was shown to block propagation of tau pathology and improve cognition in a mouse model of Alzheimer's disease (Yanamandra *et al.*, 2013).

The amyloid cascade hypothesis (Selkoe, 1991; Hardy *et al.*, 2002) suggests the appearance of tau pathology is downstream from the deposition of amyloid-β plaques. This hypothesis is supported both by findings that mutations increasing amyloid-β are sufficient to produce a genetic form of Alzheimer's disease, characterized by the presence of both neuritic plaques and tau neurofibrillary tangles, whereas mutations increasing tau may result in dementia, but do not produce an Alzheimer's disease clinical or neuropathological phenotype (Hardy *et al.*, 2002). It is also supported by CSF biomarker data suggesting changes in CSF amyloid-β can be observed earlier in the disease course than changes in CSF tau (Jack *et al.*, 2010). More recently it has been suggested that tau and amyloid-β pathology may develop independently and that amyloid-β may accelerate pre-existing tau pathology (Jack *et al.*, 2013). This hypothesis is supported both by clinical and pathological observations that tau aggregates may be found in ageing individuals in the absence of amyloid-β (Crary *et al.*, 2014) and may itself produce mild amnestic cognitive changes (a phenomenon dubbed a primary age-related tauopathy, PART). Further, numerous experiments show *in vitro*, *ex vivo* and *in vivo* manipulations that increase amyloid-β load enhance or enable both production and spread of tau pathology (Lewis *et al.*, 2001; Bolmont *et al.*, 2007). Thus, an understanding of the interaction of tau and amyloid-β in Alzheimer's disease may be critical both to understanding the course of the disease and the development of effective therapies.

The recent development of PET imaging ligands for both amyloid-β and tau represents an important advance in this direction. There are now three ^{18}F-labelled amyloid imaging agents approved for use in major international regions (Clark *et al.*, 2012; Curtis *et al.*, 2015; Sabri *et al.*, 2015). Several groups have recently reported progress in developing PET tracers for imaging tau deposition. These include a series of ^{18}F-labelled arylquinoline derivatives (Okamura *et al.*, 2013) and ^{11}C-labelled phenyl/pyridinyl-butadienyl-benzothiazoles/benzothiazoliums (Maruyama *et al.*, 2013). A third group described the 5H-pyrio[4,3-b] indole,^{18}F-T807 (subsequently known as ^{18}F-AV-1451 or flortaucipir) as a potential PET tracer for detection of tau pathology (Xia *et al.*, 2013; Chien *et al.*, 2014). *In vitro* autoradiography studies show flortaucipir binds with a dissociation constant (K_d) of 14.6 nM using brain sections from the

frontal lobe of patients with Alzheimer's disease (Xia *et al.*, 2013). Companion immunohistochemical staining showed co-localization with PHF-tau pathology but not with amyloid-β on adjacent sections, indicating that the flortaucipir autoradiography signal is most likely due to selective binding to tau pathology, although some off-target binding has been identified in midbrain regions (Marquié *et al.*, 2015). Initial clinical results with flortaucipir were reported for six subjects, including two diagnosed with Alzheimer's disease, one diagnosed with mild cognitive impairment (MCI) and three healthy control subjects (Chien *et al.*, 2014). The authors concluded there was both rapid uptake into the brain and subsequent clearance from the white matter. Inspection of standard uptake value ratio (SUVr) data from various brain regions indicated greater flortaucipir binding in Alzheimer's disease and MCI cases compared to healthy controls, particularly in the mesial and lateral temporal lobes, parietal lobe and hippocampus. This pattern of tau deposition observed by imaging was thought to be consistent with the distribution of tau pathology observed at autopsy (Braak and Braak, 1991; Braak *et al.*, 2006).

Numerous groups have since begun to explore the potential of these proposed tau PET imaging agents. Lacking a true gold standard (e.g. autopsy) for establishing that the tracers distribute in the same pattern as aggregated NFT tau in living humans, studies have focused on drawing parallels between the localization of tracer on PET imaging and the pattern of NFT accumulation thought to reflect stages of Alzheimer's disease pathology (Braak *et al.*, 2006; Brier *et al.*, 2016; Cho *et al.*, 2016*a*; Johnson *et al.*, 2016; Schöll *et al.*, 2016; Schwarz *et al.*, 2016). Studies have also noted that the distribution of tau tracer PET signal differs from the regional distribution of an amyloid PET tracer signal in the same patients (Brier *et al.*, 2016; Cho *et al.*, 2016*a*, *b*; Schöll *et al.*, 2016). Additionally, two groups have shown that flortaucipir PET signal correlates significantly with CSF tau (Brier *et al.*, 2016; Chhatwal *et al.*, 2016; Gordon *et al.*, 2016). Finally, the relationship between tau tracer PET signal and cognitive performance has also been explored. Although quantitative estimates of tau accumulation on PET imaging have been consistently higher in subjects with clinically diagnosed Alzheimer's disease dementia than in clinically normal controls (Cho, *et al.*, 2016*a*; Johnson *et al.*, 2016; Lockhart *et al.*, 2016), the degree of relationship between estimates of cortical tau and cognitive task performance has varied across studies, with some studies reporting substantial and significant correlations between neocortical SUVr and Mini-Mental State Examination (MMSE) (Okamura *et al.*, 2014; Cho *et al.*, 2016*b*; Johnson *et al.*, 2016). However, others have found no significant relationship between average cortex SUVr and cognition, but reported significant associations between regional tracer retention and specific tasks (Brier *et al.*, 2016) or specific clinical presentations across the Alzheimer's disease spectrum (Ossenkoppele *et al.*, 2016).

Together these findings provide reasonable confidence that the putative tau imaging agents in general and flortaucipir in particular may be useful for estimating density and distribution of tau pathology in patients with cognitive impairment suspected due to Alzheimer's disease. However, the studies to date have been mostly single centre studies, with modest numbers of subjects and weighted towards clinically normal subjects.

The present report expands the clinical evaluation of flortaucipir to include multicentre cross-sectional (baseline) evaluation of more than 200 subjects including young cognitively healthy controls, older controls, and patients with MCI or with possible or probable Alzheimer's disease. These subjects are part of an ongoing study that will examine the relationships between flortaucipir tau imaging, florbetapir PET amyloid status, and longitudinal cognitive deterioration.

Materials and methods

Participants

A total of 223 subjects were enrolled in this study from 25 sites. One subject did not receive a flortaucipir scan, one subject did not receive a florbetapir scan, and two subjects had technical issues (cerebellum out of field of view) with their flortaucipir scans. Additionally, two clinically-diagnosed, Aβ+ Alzheimer's disease patients with increased flortaucipir retention by visual examination were excluded; one because a large left temporal arachnoid cyst precluded use of standard temporal lobe regions of interest for purposes of quantitating flortaucipir and florbetapir retention, and another because the flortaucipir scan was started at only 63 min post-administration (planned start time is 80 min, see below), which could potentially produce an underestimation of SUVr for that subject. Thus, the 222 subjects that received flortaucipir were included in the safety analysis and 217 evaluable subjects were included for the efficacy analysis, including 16 young cognitively normal (YCN) and 58 older cognitively normal (OCN) subjects, 95 subjects with MCI, and 48 subjects with clinically-defined possible or probable Alzheimer's disease. Cognitively normal subjects had no evidence of cognitive impairment by history or examination and had a screening visit MMSE $\geqslant$ 29. YCN subjects were between 20 and 40 years of age, and OCN subjects were $>$50 years of age. MCI subjects had a diagnosis consistent with National Institute of Aging (NIA)-Alzheimer's Association criteria (MCI-Alzheimer's disease), were $>$50 years of age and had an MMSE $\geqslant$ 24. Subjects in the Alzheimer's disease group were $>$50 years of age, met NIA-Alzheimer's Association core clinical criteria for possible or probable Alzheimer's disease and had an MMSE $>$ 10. Subjects were excluded from participation if they were females of childbearing potential not using adequate contraception, had a history of stroke, current clinically significant cerebrovascular disease, drug or alcohol abuse or dependence, or if they were participating in a trial with other experimental drugs. This protocol was approved by the relevant institutional review boards and all subjects or authorized representatives signed informed consent prior to conduct of study procedures.

Results from an interim analysis of a subset of these subjects have previously been published (Schwarz *et al.*, 2016).

Assessments

All subjects underwent a clinical diagnostic interview including detailed medical history, physical and neurologic examinations, and cognitive/functional testing including MMSE, Alzheimer's Disease Assessment Scale (ADAS)-Cog, and a cognitive/functional test battery (to be reported elsewhere). An MRI performed at screening or within 6 months prior to enrolment ruled out significant CNS lesions and was used for processing of the PET images. Vital signs, laboratory values and ECG were obtained prior to and after the flortaucipir PET scans, and adverse events were monitored for 48 h post scan.

Imaging acquisition and analysis

Flortaucipir PET images used in this study were acquired for 20 min, as four 5-min frames, beginning 80 min after injection of 370 MBq flortaucipir. This uptake time was chosen based on a separate analysis of dynamic scans taken over a 0–130-min period (Shcherbinin *et al.*, 2016). On a separate day, subjects underwent a florbetapir PET scan for 10 min, as two 5-min frames, beginning 50 min after injection of 370 MBq florbetapir F18. All PET data were reconstructed with an iterative or row-action maximum likelihood algorithm with an image size of 128 × 128 or 200 × 200 matrix, pixel size of 2–2.67 mm × 2–2.67 mm, slice thickness of 2–4.25 mm, and post-reconstruction Gaussian filter of 3–5 mm or a relaxation parameter of normal or sharp filter. A T_1-weighted volumetric MRI image was also acquired.

For the florbetapir data analysis, images were spatially normalized to MNI atlas space using a florbetapir PET template in SPM (Friston *et al.*, 2007). SUVr values were calculated as an unweighted average of six cortical regions (cortical average SUVr: based on mesial orbital frontal, anterior cingulate, precuneus, posterior cingulate, parietal, and temporal) using whole cerebellum as a reference region (Joshi *et al.*, 2015). Florbetapir images were also visually interpreted by two experienced readers (M.D.D. and A.K.A.) and classified by consensus as Aβ+ or Aβ−. Readers had access to regional and global average quantitative PET scan information, which was used as an adjunct to the visual read.

For the analysis of flortaucipir PET data, the 5-min PET images were motion corrected, then summed into a single 20-min image. The summed image was then co-registered in subject space to T_1-weighted MRI image, which in turn was spatially normalized to MNI atlas space using the MNI152 T_1-weighted MRI template (Fonov *et al.*, 2009) using FSL. SPM was used to segment T_1 MRI images into probabilistic tissue maps corresponding to grey matter, white matter, and CSF. Transformations from the MRI-to-atlas spatial normalization were then used for spatial normalization of the subject-space co-registered flortaucipir PET data to MNI atlas space. For SUVr calculation, regions of interest for the individual hemispheric parcellations from the Automated Anatomical Labeling (AAL) atlas belonging to fusiform, parietal, temporal, occipital, and frontal cortical areas were used. Regions of interest near the brain periphery (parietal, temporal, occipital, frontal) were eroded using the brain boundary formed by the average atlas space T_1 MRI from all Aβ− subjects >50 years of age to reduce the likelihood of measuring activity in the extra-cortical CSF. To further reduce this likelihood, regions of interest were masked to incorporate only voxels intersecting subject grey matter tissue (tissue class likelihood >50%). Regions of interest for subcortical areas including amygdala, hippocampus, parahippocampus, fusiform, and striatum were also used. Hippocampal, parahippocampal and fusiform regions of interest were further divided into anterior and posterior subsections to permit measurement of flortaucipir focal uptake in these areas. Note, due to the relatively small size of some subcortical structures, limitations of co-registration technology and resolution of PET, the correspondence of the PET signal with the nominal AAL region may be imperfect; in particular, the hippocampus region of interest may have overlapped with parts of choroid plexus and/or fornix. Additionally, because atrophy resulted in extension of the standard striatal region of interest into ventricle in many patients, this region of interest was modified to a reduced size. For the reference region, a cerebellar grey matter region derived from the cerebellar crus-taneous (cere-crus-1 region of interest from AAL) modified by translating it inferiorly by 6 mm was chosen. This modification was performed to avoid possible overlap with inferior cortical areas and supratentorial CSF.

Individual parcellations across left and right hemispheres were grouped using voxel weights during SUVr calculation (region of interest size in number of voxels was used to weight the contribution of each region of interest to this average). Finally, a composite posterior neocortical SUVr was calculated as the weighted average of temporal, parietal and occipital areas. These areas were selected based on visual examination of data from pilot trials (e.g. NCT 02051764) as being most likely to evidence specific flortaucipir retention in Aβ+ Alzheimer's disease and MCI subjects. This selection is further supported by an interim analysis of a subset of these subjects, which indicated that the earliest/most commonly affected areas were the temporal cortex and posterior regions (Schwarz *et al.*, 2016), and are also consistent with the observations of other groups using this tracer (Johnson *et al.*, 2016) and other tracers (Okamura *et al.*, 2014). Voxel-wise SUVr images were also created, with voxels normalized to the same reference region described above. Mean images were created by averaging the voxel-wise images grouped by diagnostic cohort and florbetapir PET visual interpretation amyloid status (Aβ+ or Aβ−).

Statistical methods

Descriptive statistics were applied to summarize the subjects' demographic and baseline cognitive status by clinical diagnostic group. ANOVA with pair-wise comparisons was applied to evaluate differences among continuous variables, and χ^2 tests were applied to evaluate difference of categorical variables across diagnosis groups. Subjects were further classified by amyloid status (Aβ+, Aβ−) according to expert visual reads augmented by quantitative information. Analysis of covariance was used to evaluate differences in regional and average neocortical flortaucipir SUVr values across clinical diagnosis groups and amyloid status, adjusting for baseline age.

Planned contrasts within the model evaluated differences among cognitively normal subjects and those with MCI and Alzheimer's disease by amyloid status (i.e. within the Aβ+, or Aβ− subgroups). Similarly, the flortaucipir SUVr values were

also compared within each diagnostic group (i.e. Alzheimer's disease, MCI, or OCN) according to amyloid status through planned contrasts. YCN were not included in this model to better evaluate the effect of age exclusively among the older subjects. However a two sample *t*-test was conducted to evaluate possible differences in regional flortaucipir SUVr and neocortical average flortaucipir SUVr between the Aβ− OCN and YCN groups. The relationship between normal ageing and flortaucipir was evaluated using Pearson correlation, within the Aβ− OCN group.

A mixed effect model was used to assess the relationship of cognitive function with age, florbetapir SUVr, and flortaucipir SUVr values. MMSE or ADAS 11 score was used as the dependent variable in this model. The fixed effects included clinical diagnosis, age, florbetapir SUVr, flortaucipir SUVr, and all possible two-way and three-way interaction terms among these three variables. The random effect includes intercept. All analyses were conducted using SAS windows version 9.4. Due to the exploratory purpose of this study, no multiplicity adjustments were made during analyses.

Results

Table 1 shows the demographics and baseline characteristics for the 217 subjects with valid flortaucipir and florbetapir ^{18}F PET scans. Cognitive status was assessed by MMSE values, which ranged from a low of 12 in the Alzheimer's disease group to a high of 30 in the MCI and cognitively normal groups. The Alzheimer's disease group was significantly older than the MCI ($P = 0.02$)

Table 1 Demographic and baseline characteristics

	AD ($n = 48$)	MCI ($n = 95$)	OCN ($n = 58$)	YCN ($n = 16$)	Total population ($n = 217$)
Age (years)					
Mean (SD)	74.2 (8.79)[a]	70.4 (8.98)	68.5 (10.29)	28.9 (4.88)	67.7 (14.33)
Median	73	71	69	27.5	71
Min, max	54, 95	50, 92	50, 87	21, 39	21, 95
Gender					
Female (%)	27 (56.3)	48 (50.5)	26 (44.8)	7 (43.8)	108 (49.8)
Male (%)	21 (43.8)	47 (49.5)	32 (55.2)	9 (56.3)	109 (50.2)
Race					
Black or African (%)	2 (4.2)	7 (7.4)	9 (15.5)	3 (18.8)	21 (9.6)
Caucasian (%)	44 (91.7)	86 (90.5)	47 (81)	11 (68.8)	188 (86.6)
Native American/Alaskan (%)	1 (2.1)	0	0	0	1 (0.5)
Asian (%)	0	1 (1.1)	1 (1.7)	1 (6.3)	3 (1.4)
Other (%)	1 (2.1)	1 (1.1)	1 (1.7)	1 (6.3)	4 (1.8)
Education (years)					
Mean (SD)	15.3 (2.42)	15.8 (2.94)	15.7 (1.9)	16.6 (1.79)	15.7 (2.51)
Median	16	16	16	16	16
Min, max	6, 18	8, 27	12, 20	12, 19	6, 27
MMSE					
Mean (SD)	22.1 (3.72)[b]	27.8 (1.79)	29.5 (0.5)	29.6 (0.51)	27.1 (3.51)
Median	23	28	30	30	29
Min, max	12, 28	24, 30	29, 30	29, 30	12, 30
ADAS					
Mean (SD)	19.8 (7.95)[b]	10.3 (4.50)	5.7 (3.33)	4.1 (2.54)	10.7 (7.37)
Median	19	9	6	4	8
Min, max	8, 47	3, 24	1, 18	1, 10	1, 47
Years since diagnosis					
n	40	82	35	13	122
Mean (SD)	2.3 (2.78)	1.6 (2.02)	N/A	N/A	1.9 (2.31)
Median	1.2	0.9	N/A	N/A	1.0
Min, max	0.0, 12.6	0.0, 10.9	N/A	N/A	0.0, 12.6
Florbetapir SUVr					
Mean (SD)	1.31 (0.32)[b]	1.19 (0.25)	0.97 (0.14)	0.91 (0.07)	1.13 (0.27)
Median	1.37	1.15	0.95	0.91	1.01
Min, Max	0.80, 1.83	0.79, 1.78	0.82, 1.71	0.81, 1.01	0.79, 1.83
Florbetapir positive (%)	32 (66.7)	46 (48.4)	5 (8.6)	0	83 (38.2)

AD = Alzheimer's disease; SD = standard deviation.

[a]Alzheimer's disease group significantly older than the MCI ($P = 0.02$) and OCN groups ($P = 0.003$).

[b]Alzheimer's disease group significantly different than MCI and cognitively normal groups ($P < 0.0001$).

and OCN groups ($P = 0.003$) and had significantly lower MMSE and higher (more impaired) ADAS scores than the MCI or the cognitively normal groups ($P < 0.0001$). Although there were no significant differences in education across diagnostic groups, these were highly educated subjects with a mean of nearly 16 years of schooling completed. Mean florbetapir PET SUVr values were higher in the Alzheimer's disease and MCI group than in the YCN or OCN group ($P < 0.0001$); florbetapir PET was classified as Aβ+ for 32/48 (66.7%) Alzheimer's disease, 46/95 (48.4%) MCI, 5/58 (8.6%) OCN, and 0/16 (0%) YCN subjects (Fishers exact test comparing percentages across diagnostic groups; $P < 0.0001$).

Analysis of safety

A total of 43 adverse events affecting 32 individual subjects were reported; none were considered serious. The most common adverse events were injection site pain ($n = 7$, 3.2%), elevations in blood pressure as measured from pre-administration to post-scan ($n = 6$, 2.7%), headache ($n = 3$, 1.4%), paraesthesia ($n = 2$, 0.9%), and fatigue ($n = 2$, 0.9%). No other adverse events occurred more than once per subject, and none were more than moderate in intensity.

Flortaucipir image results

Figure 1 shows flortaucipir voxel-wise SUVr images averaged across subjects within diagnostic cohort as a function of amyloid status (visual interpretation: Aβ+ or Aβ−). The mean images suggest that little focal retention of flortaucipir occurred in YCN other than possibly a slight elevation in the midbrain/brainstem (Fig. 1A). On average, Aβ− OCN showed no focal cortical retention but the mean image showed increased flortaucipir retention in midbrain, striatum and some mesial temporal lobe regions, particularly in the amygdala and hippocampus/choroid plexus region. The pattern of flortaucipir retention in Aβ− clinically diagnosed MCI or Alzheimer's disease subjects was similar to that for Aβ− OCN, with no focal retention in cortical areas, but elevated retention in striatum, hippocampus/choroid plexus and brainstem. The pattern of retention in Aβ+ OCN was similar to that for Aβ− OCN, with the exception of slightly increased retention in the amygdala and hippocampus region of interest with some spread to isocortical areas, particularly lateral temporal cortex in some subjects. The density and area of affected cortical regions further increased in Aβ+ MCI and further still in Aβ+ Alzheimer's disease subjects (Fig. 1B).

Figure 2 shows tracer retention in representative individual young and older Aβ− cognitively normal and in Aβ+ OCN, MCI, and Alzheimer's disease subjects. The tracer retention in individual Aβ+ subjects was consistent with the pattern described above, in that the lateral temporal lobes appeared to be the first and most common area affected in individuals. However, there was considerable variability in extent and laterality of affected areas in individual subjects, with some Aβ+ subjects showing flortaucipir retention limited to focal regions of the temporal lobe, and others showing widespread distribution to posterior regions and in some cases frontal lobes. In some cases flortaucipir distribution was symmetrical, but in other cases flortaucipir retention was markedly greater in one hemisphere than the other. In addition, there were also differences across Aβ+ subjects with respect to the relative intensities in limbic versus cortical regions (e.g. Fig. 2D row 1 versus 3) that may reflect varying patterns of tau distribution recently noted in the pathology literature (Murray *et al.*, 2011).

To obtain quantitative estimates of flortaucipir retention, regional and composite SUVr values were obtained. Table 2 shows mean and standard deviation for SUVr values for representative regions as well as nominal statistical probabilities for group comparisons as a function of diagnostic cohort and amyloid status.

Similarly, analysis of covariance with planned contrasts to compare groups of interest showed no differences in regional or composite posterior neocortical SUVr as a function of diagnosis among Aβ− clinically diagnosed Alzheimer's disease, MCI and OCN. However, for Aβ+ subjects, flortaucipir neocortical SUVr increased across diagnostic groups (Alzheimer's disease > MCI > OCN) and was consistently elevated for Aβ+ MCI and Alzheimer's disease subjects relative to the respective Aβ− subjects (Table 2).

There were no differences in regional or average neocortical SUVr between the Aβ− OCN and YCN groups. However, Aβ− OCN subjects showed age-related increases in flortaucipir SUVr as evidenced by a difference in SUVr between YCN and Aβ− OCN that reached the nominal level of significance in the striatum ($P = 0.0001$), amygdala ($P = 0.002$) and anterior hippocampus/choroid plexus ($P = 0.013$) regions of interest. Looking only within the Aβ− OCN group, there was also a significant correlation between age and SUVr ($r = 0.33$, and 0.36 for anterior hippocampus/choroid plexus and striatum, respectively, $P < 0.02$).

Figure 3 shows a scatter plot of SUVr averaged across representative cortical regions for individual subjects in the different diagnostic categories. Consistent with the statistical analysis above, Aβ− subjects had consistently low composite posterior cortical flortaucipir SUVr. Subjects with high composite posterior neocortical flortaucipir SUVr (outside the upper 99% confidence limits for YCN, dashed line) were predominantly Aβ+. However, it is clear that a significant proportion of Aβ+ subjects also had posterior cortical average SUVr that fell within the range of controls. Upon visual review of these images, many exhibited focal and/or unilateral flortaucipir uptake in neocortical regions, especially lateral temporal lobe (Fig. 4), a pattern that was rare, albeit not always absent, in Aβ− subjects.

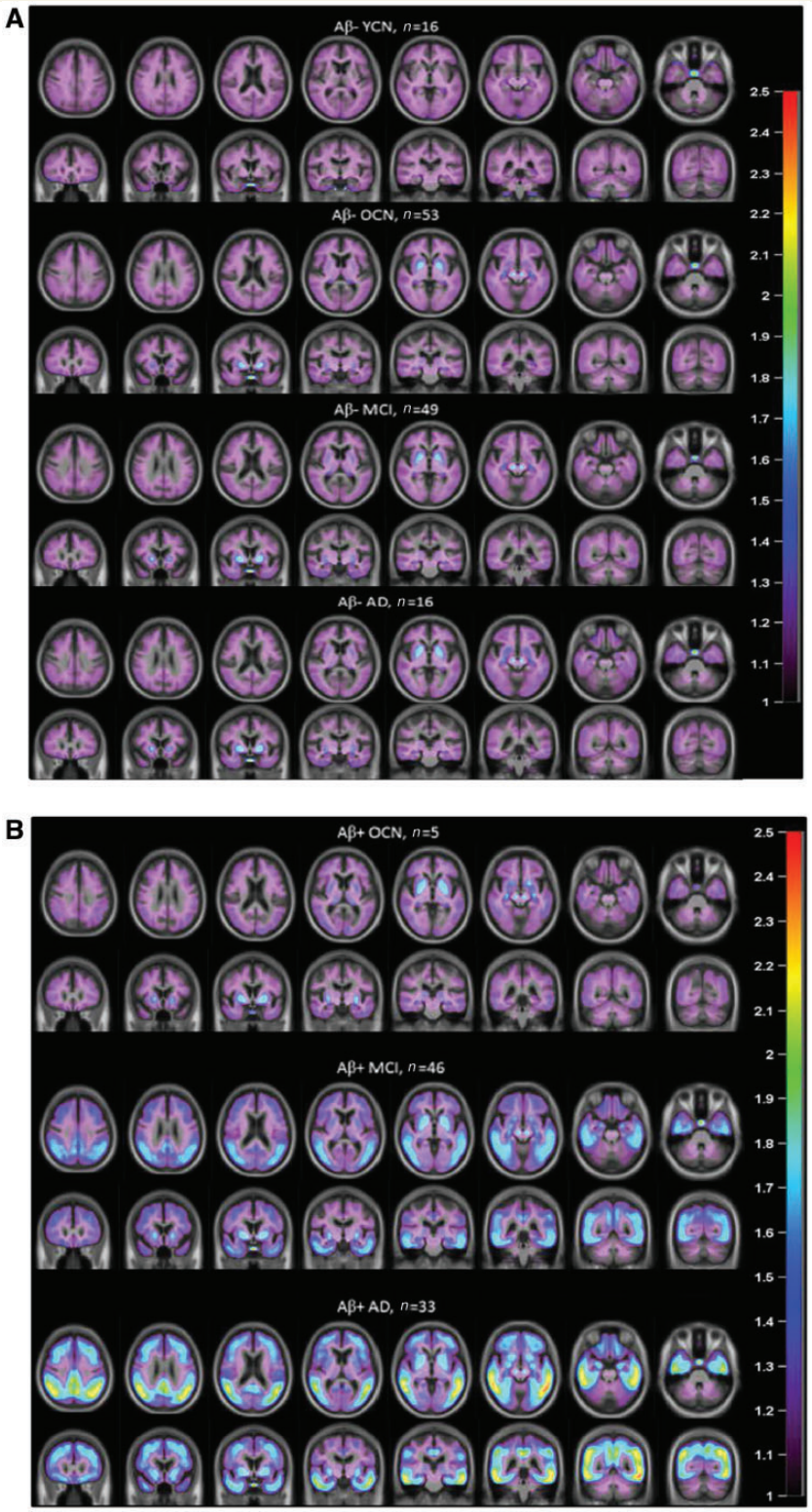

Figure 1 Mean flortaucipir voxel-wise SUVr images for each age/diagnostic cohort by florbetapir PET amyloid status (Aβ+ or Aβ−). Images are scaled from 1–2.5 SUVr units and overlaid on an average of MRI from all study patients in radiologic orientation such that the right side of each image represents left hemisphere of the brain. (**A**) Aβ−; (**B**) Aβ+. AD = Alzheimer's disease; ROI = region of interest.

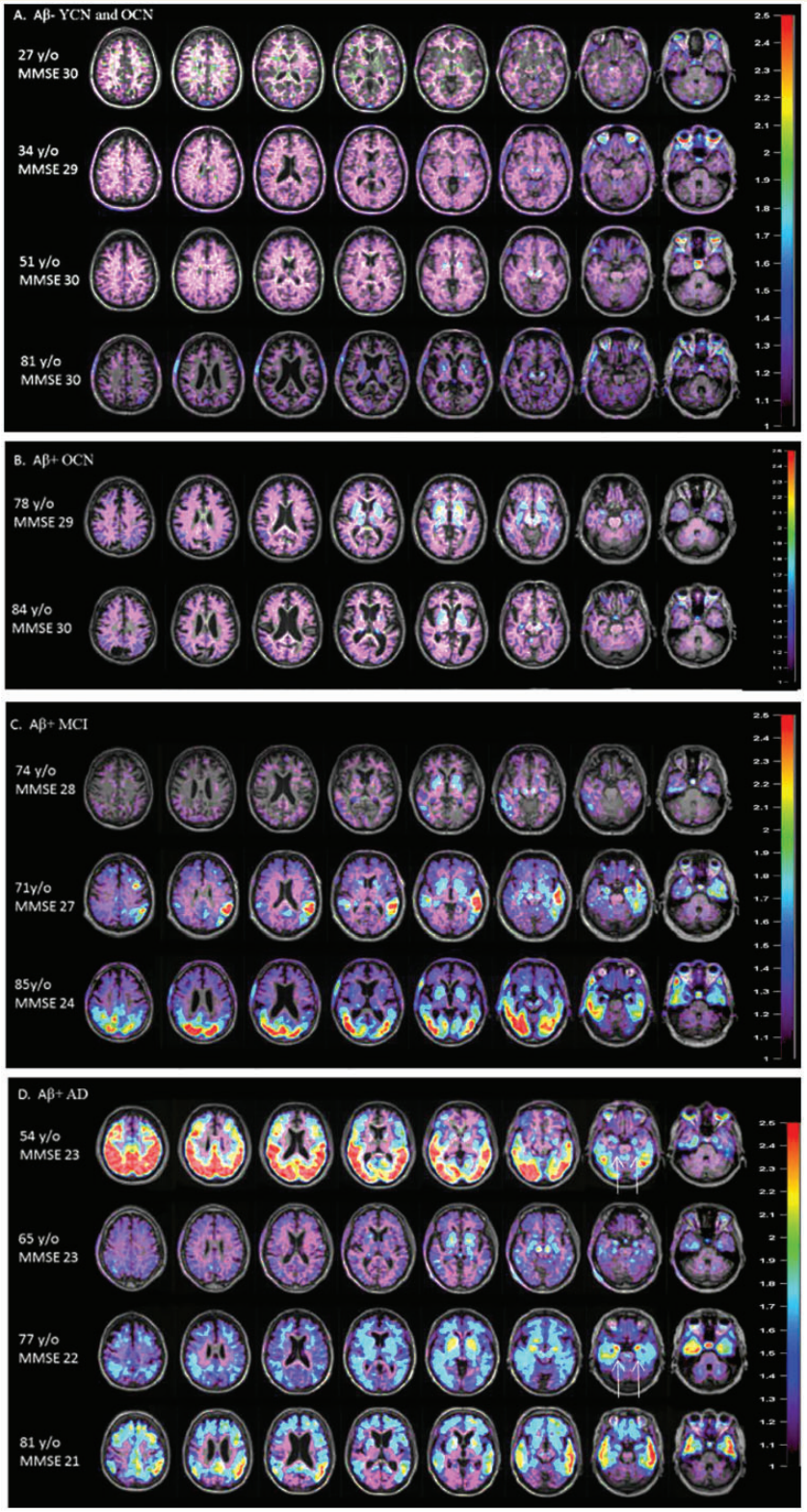

Figure 2 Flortaucipir voxel-wise SUVr images for representative individual Aβ− control (YCN/OCN) and Aβ+ OCN, MCI, and Alzheimer's disease subjects. (**A**) Aβ− control (YNC/OCN), (**B–D**) Aβ+ OCN, MCI and Alzheimer's disease subjects, respectively. PET images are scaled from 1–2.5 SUVr units and overlaid on each subject's respective MRI. Note in addition to differences in overall extent of retention, there are also subjects with relatively limbic sparing (**D**, *first row*) and limbic predominant (**D**, *third row*) patterns (arrows) consistent with the pathology literature (Murray *et al.*, 2011). AD = Alzheimer's disease; y/o = years old.

Table 2 Composite posterior cortical and regional, mean (SD), flortaucipir SUVr by clinical diagnostic cohort and amyloid status

Region	AD *n* = 48; 33 Aβ+	MCI *n* = 95; 46 Aβ+	OCN *n* = 58; 5 Aβ+	YCN *n* = 16	Group comparison *P* < 0.05*
Cortical average combination region of interest					
Aβ+ SUVr	1.55 (0.352)	1.36 (0.377)	1.09 (0.061)		AD > OCN; AD > MCI; MCI > OCN
Aβ− SUVr	1.07 (0.083)	1.05 (0.082)	1.07 (0.085)	1.09 (0.062)	
P§: Aβ+ versus Aβ−	<0.0001	<0.0001	0.3662		
Frontal					
Aβ+	1.39 (0.417)	1.21 (0.354)	0.99 (0.137)		AD > OCN; AD > MCI
Aβ−	0.99 (0.114)	0.98 (0.090)	1.00 (0.095)	1.04 (0.083)	
P§: Aβ+ versus Aβ−	<0.0001	<0.0001	0.4568		
Occipital					
Aβ+	1.43 (0.310)	1.32 (0.386)	1.08 (0.025)		AD > OCN; AD > MCI
Aβ−	1.08 (0.088)	1.06 (0.081)	1.08 (0.085)	1.11 (0.067)	
P§: Aβ+ versus Aβ−	<0.0001	<0.0001	0.6004		
Parietal					
Aβ+	1.60 (0.466)	1.33 (0.430)	1.07 (0.081)		AD > OCN; AD > MCI
Aβ−	1.03 (0.101)	1.02 (0.092)	1.03 (0.091)	1.07 (0.072)	
P§: Aβ+ versus Aβ−	<0.0001	<0.0001	0.2569		
Temporal					
Aβ+	1.64 (0.403)	1.42 (0.373)	1.11 (0.091)		AD > OCN; AD > MCI; MCI > OCN
Aβ−	1.09 (0.085)	1.08 (0.089)	1.10 (0.091)	1.10 (0.060)	
P§: Aβ+ versus Aβ−	<0.0001	<0.0001	0.3814		
Amygdala					
Aβ+	1.48 (0.185)	1.35 (0.204)	1.23 (0.119)		AD > OCN; AD > MCI
Aβ−	1.24 (0.235)	1.14 (0.137)	1.13 (0.117)	1.03 (0.096)	AD > OCN; AD > MCI; OCN > YCN
P§: Aβ+ versus Aβ−	<0.0001	<0.0001	0.2245		
Anterior hippocampus					
Aβ+	1.43 (0.207)	1.35 (0.186)	1.25 (0.171)		AD > OCN
Aβ−	1.21 (0.203)	1.17 (0.149)	1.17 (0.143)	1.07 (0.110)	OCN > YCN
P§: Aβ+ versus Aβ−	<0.0001	<0.0001	0.3409		
Posterior hippocampus					
Aβ+	1.29 (0.184)	1.32 (0.179)	1.27 (0.160)		
Aβ−	1.19 (0.215)	1.26 (0.193)	1.26 (0.193)	1.17 (0.145)	
P§: Aβ+ versus Aβ−	0.1074	0.1747	0.8572		
Anterior parahippocampal					
Aβ+	1.49 (0.243)	1.32 (0.245)	1.07 (0.135)		AD > OCN; AD > MCI; MCI > OCN
Aβ−	1.12 (0.204)	1.03 (0.151)	1.04 (0.106)	1.02 (0.085)	
P§: Aβ+ versus Aβ−	<0.0001	<0.0001	0.5698		
Posterior parahippocampus					
Aβ+	1.40 (0.197)	1.29 (0.203)	1.12 (0.128)		AD > OCN; AD > MCI; MCI > OCN
Aβ−	1.10 (0.151)	1.10 (0.132)	1.09 (0.113)	1.07 (0.098)	
P§: Aβ+ versus Aβ−	<0.0001	<0.0001	0.5642		
Fusiform					
Aβ+	1.66 (0.347)	1.47 (0.370)	1.15 (0.104)		AD > OCN; AD > MCI; MCI > OCN
Aβ−	1.16 (0.109)	1.11 (0.106)	1.12 (0.103)	1.11 (0.076)	
P§: Aβ+ versus Aβ−	<0.0001	<0.0001	0.6271		
Striatum					
Aβ+	1.28 (0.153)	1.28 (0.155)	1.25 (0.239)		
Aβ−	1.18 (0.174)	1.19 (0.171)	1.20 (0.189)	1.00 (0.120)	OCN > YCN
P§: Aβ+ versus Aβ−	0.1269	0.0567	0.9579		

AD = Alzheimer's disease.

*P-value < 0.05: pair-wise comparisons through planned contrasts within the ANCOVA model, adjusting for age. Planned contrasts included differences among OCN subjects and MCI or Alzheimer's disease within amyloid status groups (Aβ+ or Aβ−; rows) and differences in flortaucipir SUVR values across amyloid status for each diagnostic group (Alzheimer's disease, MCI, and OCN; columns). A separate, independent two-group *t*-test compared OCN versus YCN. Corrections for multiple comparisons were not performed. Exact *P*-values can be found in Supplementary Table 1.

§*P*-values comparing Aβ+ versus Aβ−.

Figure 4 shows four representative Aβ+ clinically diagnosed Alzheimer's disease subjects with flortaucipir neocortical average SUVr in the range of young controls. The first three subjects are examples of subjects with tracer retention in lateral temporal lobe of at least one hemisphere that was elevated beyond that typically seen in Aβ− clinically normal subjects (*cf.* Fig. 2A).

Both tau and amyloid-β density, as measured by flortaucipir and florbetapir SUVr values, respectively, independently correlated with cognitive performance on MMSE (flortaucipir SUVr: $r = -0.42$, $P < 0.0001$; florbetapir SUVr: $r = -0.47$, $P < 0.0001$) and ADAS (flortaucipir SUVr: $r = 0.45$, $P < 0.0001$; florbetapir SUVr: $r = 0.49$, $P < 0.0001$). There was also a significant correlation between flortaucipir and florbetapir SUVr ($r = 0.64$, $P < 0.0001$) and among the Aβ+ subjects, a significant inverse correlation between flortaucipir SUVr and age ($r = -0.48$, $P < 0.0001$). However, when combined in a mixed model with clinical diagnosis and age as predictors of MMSE or ADAS, none of the factors besides clinical diagnosis achieved significance (Supplementary Table 2)

These relationships are represented graphically in Fig. 5. Figure 5A shows the relationship between florbetapir and flortaucipir SUVr. As previously described (Fig. 3), Aβ− florbetapir PET scans were consistently associated with low flortaucipir SUVr. While Aβ+ florbetapir PET scans were not always associated with elevated flortaucipir SUVr, the probability of an elevated flortaucipir SUVr increased as a function of florbetapir SUVr. Figure 5B shows the relationship between flortaucipir SUVr and age for both Aβ− and Aβ+ subjects. As noted above, Aβ− subjects had low posterior neocortical average flortaucipir SUVr regardless of age, whereas Aβ+ subjects had increased SUVr compared to controls, but showed an age-related decrease in flortaucipir SUVr. Finally, Fig. 5C and D shows the relationship between flortaucipir SUVr and ADAScog11 error score for Aβ+ subjects under 75 and over 75, respectively. Although the relationship between flortaucipir SUVr and ADAS was significant in both groups ($P = 0.0039$ and $P = 0.0443$, respectively), examination of the scatter plots shows that in the younger (<75 years) cohort, the demented subjects consistently showed elevated flortaucipir SUVr (>1.25, beyond the range of young controls), and the strength of relationship between flortaucipir SUVr and ADAS was limited primarily by a group of MCI subjects with high flortaucipir SUVr despite limited cognitive impairment. In contrast, approximately half of the demented patients over 75 years of age had relatively low flortaucipir SUVr despite substantial cognitive impairment. Visual examination of mean voxel-wise SUVr images from these >75-year-old subjects reveals flortaucipir retention in essentially the same regions as in the under 75 year olds, but with a lessor density. Thus, the mean images from the Aβ+ over 75 year old Aβ+ demented subjects most resemble the images from the Aβ+ MCI subjects less than 75 years old (Fig. 6)

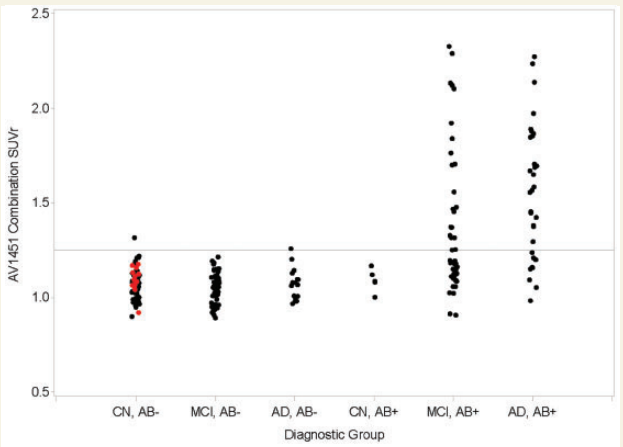

Figure 3 Posterior neocortical composite SUVr for individual subjects by diagnostic category. *X*-axis: (diagnostic group, amyloid status), YCN are shown in red. *Y*-axis: flortaucipir (AV1451) combination SUVr. Horizontal reference line shows upper 99% confidence limit for YCN. AD = Alzheimer's disease; CN = cognitively normal.

Discussion

Flortaucipir is a PET imaging agent designed to directly assess the level of aggregated tau in the brains of living patients. The present study examined the brain distribution and retention of flortaucipir in relation to florbetapir PET amyloid status (Aβ+ or Aβ−), clinical diagnosis (cognitively normal, MCI or Alzheimer's disease), age, and cognitive performance (MMSE and ADAS). In Aβ+ subjects flortaucipir neocortical SUVr increased significantly across clinical diagnostic groups (Alzheimer's disease > MCI > OCN) and was significantly elevated for Aβ+ MCI and Alzheimer's disease subjects relative to the respective Aβ− subjects. Aβ− cognitively normal subjects showed an age-related increase in tracer retention in some mesial temporal lobe regions (amygdala, hippocampus/choroid plexus) as well as presumed off-target binding in brainstem and striatum, but minimal focal cortical retention. The pattern of flortaucipir distribution and retention in Aβ− cognitively impaired (clinically diagnosed MCI and Alzheimer's disease) subjects did not differ from that in cognitively normal subjects. The pattern of flortaucipir distribution among Aβ+ subjects was reminiscent of the cross-sectional distribution of tau reported in post-mortem pathology studies (Braak and Braak, 1991, Braak *et al.*, 2006), in that the most commonly affected regions were in the temporal lobe. This is also where the first signs of increased retention appeared in Aβ+ cognitively normal subjects, though with only five subjects in this group, the relatively mild changes seen in this group should be considered with caution. Further increases in density and a wider cortical distribution were observed on average in

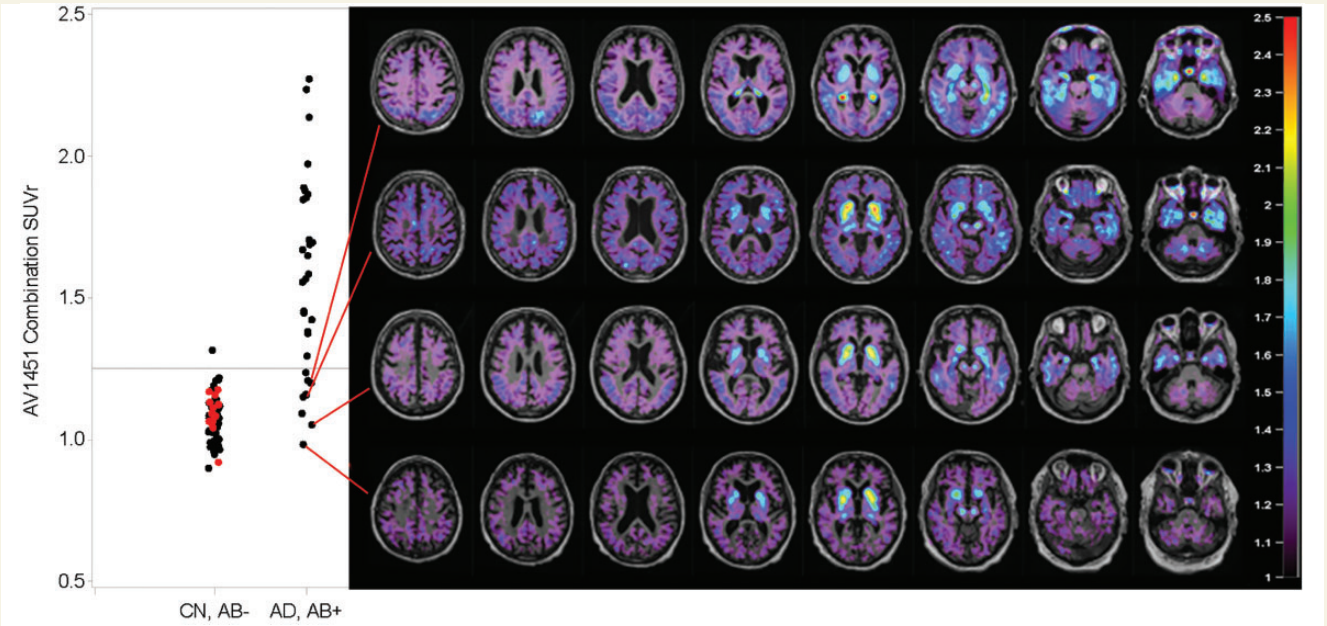

Figure 4 Aβ+ subjects with low cortical average SUVR values. Subjects with low flortaucipir SUVr values may still have abnormal tracer retention in limited cortical regions. AD = Alzheimer's disease; CN = cognitively normal; ROI = region of interest.

the Aβ+ MCI and Alzheimer's disease groups. However, there was significant variability in extent and density of flortaucipir tau binding among the Aβ+ subjects. Elevated flortaucipir tau binding was associated with an increased prevalence of cognitive impairment as assessed by MMSE and ADAS, especially in subjects under the age of 75.

These results are consistent with the hypothesis (Jack *et al.*, 2013) that tau and amyloid pathology may begin independently, but that spread of tau beyond mesial temporal lobe is associated with, and may be dependent, on amyloid accumulation. Further, the results are consistent with the hypothesis that cortical tau may be associated with neuronal dysfunction and associated cognitive impairment.

Approximately a third of the demented subjects and half of the MCI subjects in this study were Aβ− based on the florbetapir scan interpretation. The relatively high proportion of Aβ− subjects, particularly in the demented group, may be in part a consequence of the inclusion of clinically defined possible, as well as probable Alzheimer's disease cases. The finding of low focal cortical flortaucipir retention in these Aβ− subjects is consistent with the interpretation that a negative florbetapir scan indicates the absence of Alzheimer's disease and thus, the absence of Alzheimer's disease-related tau deposition (hence low cortical flortaucipir retention). Interestingly increased mesial temporal lobe flortaucipir SUVr was observed with age even in these Aβ− subjects. It is possible that some of this signal could represent spill out from flortaucipir binding in the choroid plexus. This may represent binding to abnormal tau aggregation (Ikonomovic *et al.*, 2016) but it could also reflect off target binding (Lowe *et al.*, 2016), alternatively the elevated SUVr in the hippocampus/choroid plexus region of interest may reflect age-related aggregation of tau in the mesial temporal lobe, the pathologically defined syndrome of primary age-related tauopathy (PART, Crary *et al.*, 2014).

Although elevated flortaucipir in the composite posterior cortical SUVr was consistently associated with a positive amyloid PET scan, not all Aβ+ subjects showed an elevated composite posterior cortical SUVr. Visual examination of images from Aβ+ subjects with lower posterior neocortical composite flortaucipir SUVr suggested that many, but not all, had focal retention in lateral temporal cortex beyond the level seen in cognitively normal controls. Longitudinal studies are required to determine whether the presence of focal tau accumulation in the lateral temporal cortex represents an early stage of Alzheimer's disease (e.g. Braak III), as might be suggested from comparison to the pathology literature (Schwarz *et al.*, 2016) or some non-Alzheimer's disease tauopathy, or whether it simply reflects image noise. It also remains to be determined whether all Aβ+ subjects eventually show increased retention in lateral temporal lobe and whether Aβ+ subjects with low/focal flortaucipir retention are at increased risk for future spread of neuropathological tau (as represented by flortaucipir) resulting in progressive cognitive impairment.

These questions may have important implications for future clinical trials of anti-Alzheimer's disease therapeutic agents. Previous results showing that subjects who have a clinical profile of MCI due to Alzheimer's disease or

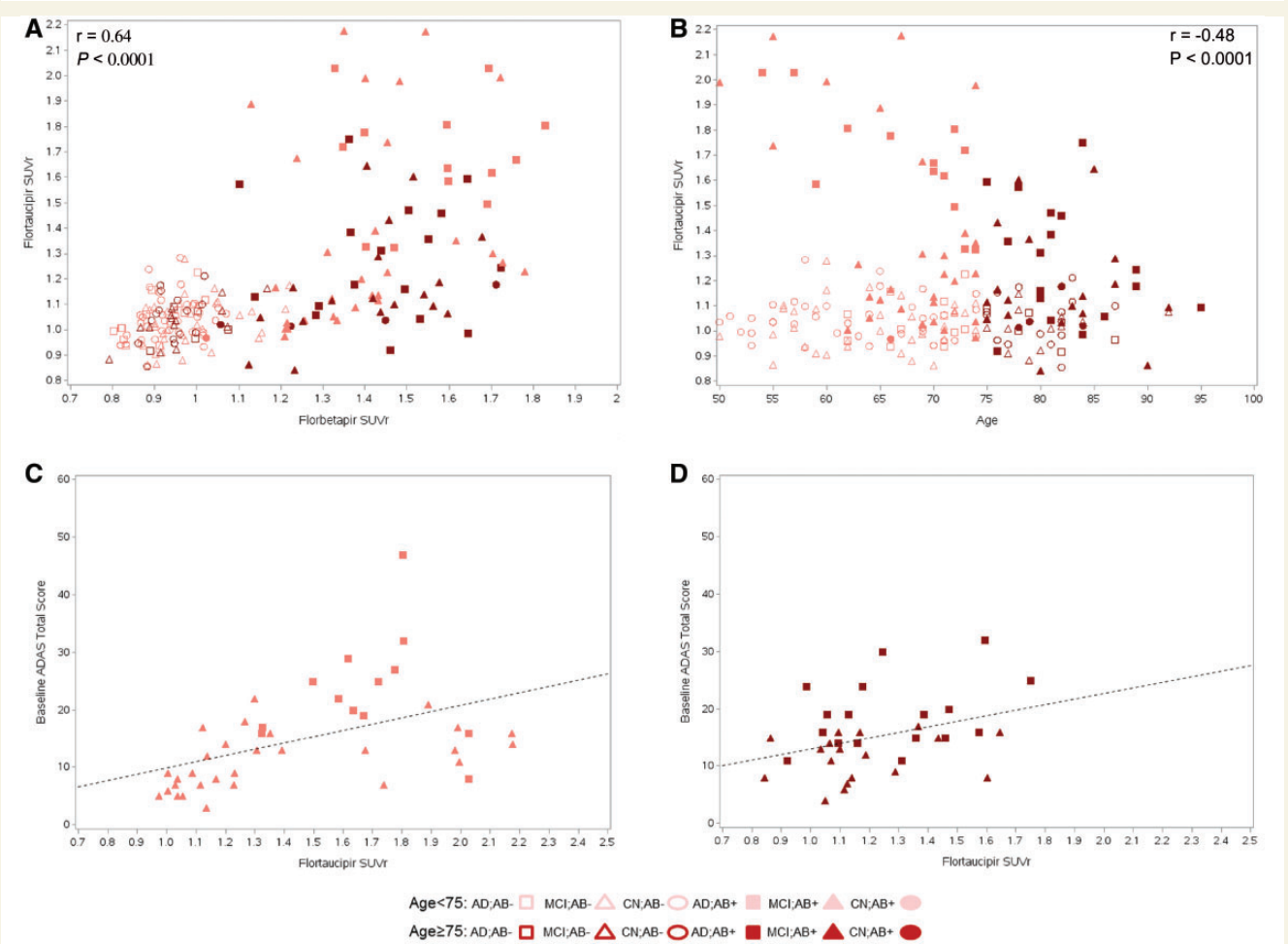

Figure 5 Relationship between florbetapir PET SUVr, flortaucipir SUVr, diagnosis, age and ADAS score. (**A**) Scatterplot of relationship between florbetapir and flortaucipir SUVr for individual subjects by age, diagnosis and amyloid status. (**B**) Scatterplot of relationship between age and flortaucipir SUVr for individual subjects by age, diagnosis and amyloid status (r and *P*-values refer to Aβ+ subjects only). (**C** and **D**) Scatterplot of relationship between flortaucipir SUVr and cognition for individual subjects by diagnosis and amyloid status and age (<75 years, **C**; >75 years **D**). AD = Alzheimer's disease; CN = cognitively normal.

probable Alzheimer's disease and who are Aβ− (thus inconsistent with Alzheimer's disease) deteriorate at a slower rate than subjects who are Aβ+ (Doraiswamy, 2012, 2014) have led to amyloid status assessment as a screening procedure for most phase III clinical trials. The present finding that Aβ+ subjects may differ in tau density and distribution, despite similar MMSE scores at baseline, raises additional considerations. Will Aβ+ patients with low tau deteriorate at different rates than subjects with high density/widespread distribution of tau and how might this affect study power? Is there an optimal range of tau (disease stage) for treatment with anti-amyloid or anti-tau therapies? Ongoing longitudinal follow-up may shed further light on these questions.

The pattern of tracer retention in the present study is consistent with and extends previous findings (Chien *et al.*, 2014; Cho *et al* 2016 *a*, *b*; Johnson *et al.*, 2016; Schöll *et al.*, 2016; Schwarz *et al.*, 2016) to a larger sample including both Aβ+ and Aβ− mildly-impaired and demented subjects. Also consistent with previous reports, the variation in flortaucipir retention in the present study was associated with variation in degree of cognitive impairment across all subjects and also within the Aβ+ subgroup. As a group, Aβ+ subjects with elevated composite posterior cortical SUVr were at increased risk for dementia and for cognitive impairment, as evidenced by MMSE or ADAS scores (Fig. 5). This relationship was even clearer in subjects under the age of 75 than in the study as a whole. Whereas some

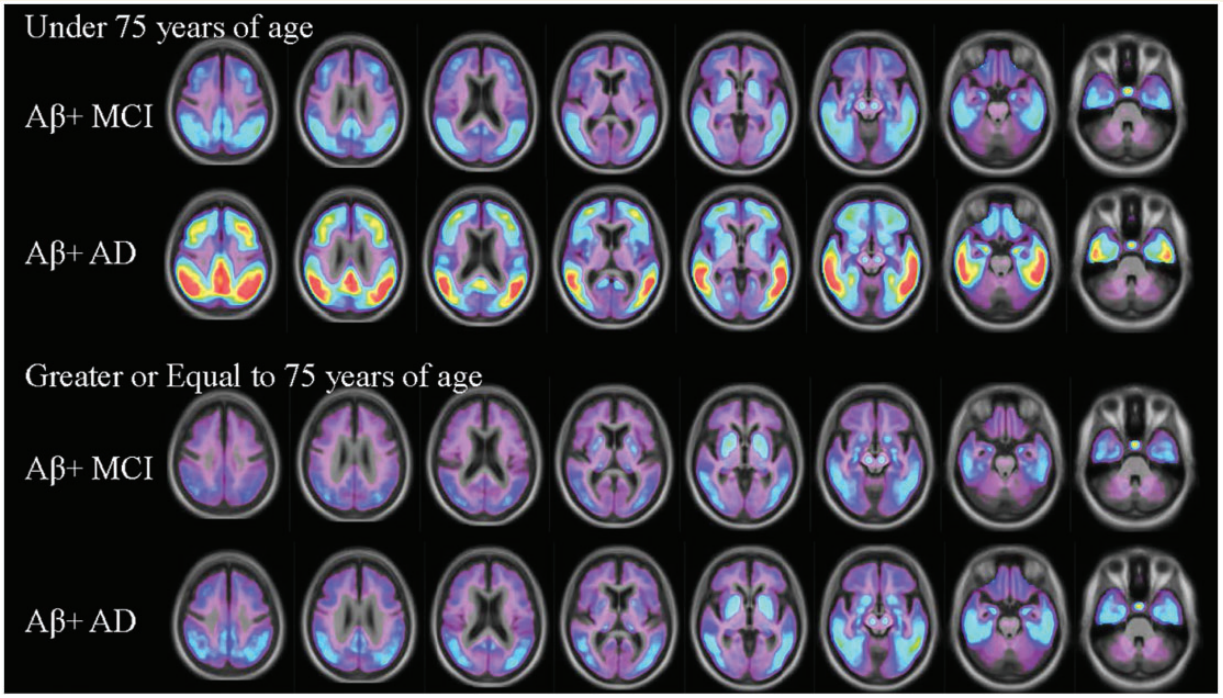

Figure 6 Mean flortaucipir voxel-wise SUVr images for Aβ+ MCI and Alzheimer's disease subjects <75 years and ⩾75 years old. Note the similarity between the pattern of demented (Alzheimer's disease) subjects ⩾75 years to MCI subjects <75 years of age. AD = Alzheimer's disease.

older individuals carried diagnoses of Alzheimer's disease or had significant impairment based on MMSE/ADAS scores despite low posterior cortical average flortaucipir retention, this was rare in subjects under the age of 75. This contrast of tau distribution between under 75 and over 75 aged subjects has not previously been reported in PET imaging studies, perhaps due to the small number of impaired patients in previous studies. However, these results are in agreement with pathology reports that show reduced correlation between level of tau and dementia in the 'oldest old' compared to younger patients (Prohovnik *et al.*, 2006; Middleton *et al.*, 2011). The most likely explanation is that in older individuals, Alzheimer's disease-related cognitive impairments may be exacerbated by age-related neurodegeneration and other pathologies, such as Lewy bodies or TAR DNA-binding protein 43 (TDP-43, encoded by *TARDBP*) inclusions, or comorbidities such as cardiovascular or cerebrovascular disease. Conversely, younger subjects may be relatively free of other pathologies and hence may be able to sustain a higher load of Alzheimer's disease pathology at the same level of cognitive impairment (*cf.* <75 years MCI versus >75 years Alzheimer's disease in Fig. 6).

This hypothesis is consistent with recent biomarker findings (Jack *et al.*, 2016) suggesting that the incidence of neurodegenerative disease in the absence of amyloidosis increases more than 10-fold between ages 65 and 85, whereas incidence of amyloidosis in the absence of neurodegeneration shown by MRI and FDG PET biomarkers peaks between ages 60 and 75. Together these results suggest a model of Alzheimer's disease wherein mesial temporal tau and other neuropathologic insults, as evidenced by MRI or FDG PET, begin independently, with an increasing likelihood as a function of age. The onset of amyloidosis amplifies this impact by enabling the spread of tau beyond the mesial temporal lobe, resulting in the neuronal dysfunction and cognitive impairment associated with Alzheimer's disease. Amyloid-enabled tau spread may add to or uncover deficits resulting from non-Alzheimer's disease related pathologies, so that the magnitude of cognitive deficit may be due to both the degree of concomitant pathology and the density and spread of tau.

It is still unclear how amyloid enables the spread of tau through neocortical regions. *In vitro* studies have shown that amyloid-β aggregates can cross-seed tau aggregates (Vasconcelos *et al.*, 2016) and *in vivo* studies have shown that intracerebral injection of aggregated amyloid-β can enhance both the expression of tau aggregates in hippocampus and the spread of tau from hippocampus to cortex of transgenic mice (Bolmont *et al.*, 2007). However, both histopathology studies in autopsy tissue (Braak and Braak, 1991) and recent PET imaging studies with amyloid and tau tracers (Brier *et al.*, 2016; Cho *et al.*, 2016*a*; Schöll *et al.*, 2016) suggest an incomplete overlap in the pattern of distribution of amyloid and Alzheimer's disease. In PET studies, deposition of amyloid appears to occur roughly simultaneously across multiple brain areas with the greatest concentrations in frontal cortex and medial parietal cortex

(precuneus, posterior cingulate), whereas tau deposition is seen most often in, and may be largely limited to the temporal cortex, at a time when the amyloid PET scan shows widespread neocortical amyloid. Thus, local neocortical density of amyloid does not appear to necessarily translate into local tau accumulation. Rather in both animal studies (Bolmont *et al.*, 2007; Pooler *et al.*, 2014) and in the present and other tau PET imaging studies (Brier *et al.* 2016; Cho *et al.*, 2016 *a*, *b*; Schöll *et al.*, 2016), elevated neocortical amyloid was associated with increased medial temporal tau accumulation, followed at later stages of disease by a hierarchical spread to lateral temporal and other neocortical regions. Longitudinal follow-up and multimodal evaluations may be valuable in further elucidating the course of this process.

This report is based on an analysis of the baseline data from an ongoing longitudinal study. As such, it has a number of important limitations, several of which have previously been mentioned. Although the present study is the largest to evaluate a tau-targeted PET imaging agent to date, the number of subjects still represents a relatively small population on which to characterize the pattern of tracer retention while accounting for factors such as age, diagnosis and amyloid status. In particular, only five OCN subjects were classified as Aβ+, and the increases in mesial and lateral temporal lobe flortaucipir uptake in these patients compared to Aβ− OCN were relatively modest. Although these results are similar to those reported recently for larger cohorts of Aβ+ clinically normal subjects (Johnson *et al.*, 2016; Schöll *et al.*, 2016), additional data are needed in this important subject group, because flortaucipir PET scans in this group of subjects could provide information on the earliest stages of Alzheimer's disease pathological changes (i.e. preclinical Alzheimer's disease, Sperling *et al.*, 2011).

It should be noted that the inclusion criteria of the present study were designed to select for subjects with Alzheimer's disease-like clinical profiles (MCI-Alzheimer's disease, possible or probable Alzheimer's disease) and excluded subjects with primary behavioural and motor deficits, such as those associated with non-Alzheimer's disease tauopathies like fronto-temporal dementia and progressive supranuclear palsy. Therefore, the present data alone are not sufficient to evaluate the sensitivity and specificity of this pattern of tracer retention for Alzheimer's disease versus other non-Alzheimer's disease tauopathies. However, the finding, in this study, that elevated posterior cortical flortaucipir SUVr was observed only in Aβ+ subjects is consistent with the hypothesis that flortaucipir retention in these areas may represent an Alzheimer's disease-specific pattern. This concept is also supported by recent *in vitro* studies that have suggested that flortaucipir may have a greater propensity for specific binding to Alzheimer's disease tissue than to other non-Alzheimer's disease tauopathies (Marquié *et al.*, 2015; Lowe *et al.*, 2016; Sander *et al.*, 2016).

Moreover, the study was exploratory by design. Although the prespecified statistical analyses have returned nominal *P*-values, we did not correct for multiple comparisons, and thus the *P*-values should be considered a guide to the reliability of the findings, rather than a formal test of hypotheses. The image analysis methods presented represent initial techniques for quantifying overall flortaucipir retention. The regions of interest employed were large and not specifically designed for sensitivity to tau accumulation. Statistically-derived regions designed to focus on voxels most likely to be sensitive to amyloid burden and/or cognitive impairment might be more useful in stratifying patients for degree of current impairment or risk for future deterioration. It may also be possible to improve on the current cerebellum reference region. Similarly, the cognitive tests reported here (MMSE, ADAS-Cog) are global measures of cognitive status. Analyses of the more specifically targeted tasks in a more extensive neuropsychological test battery are ongoing to determine if specific categories of tasks (e.g. working memory tasks) are associated with flortaucipir retention in specific brain regions or voxels.

Finally, although the pattern of flortaucipir retention across brain areas was generally, and on average, consistent with the expectation for a tau imaging compound, there was significant individual variability. There was also accumulation of tracer in some unexpected regions. Specifically, the apparent age-related retention in the striatum and midbrain was not anticipated based on the typical distribution of tau pathology in ageing and Alzheimer's disease. Although tau may accumulate in striatum in later stages of disease, it is not expected to be present in elderly normal subjects (Braak and Braak, 1991, Braak *et al.*, 2006). Kinetic analyses (Shcherbinin *et al.*, 2016) suggest that both uptake and washout of tracer in the striatum of older subjects is higher than other brain regions, particularly compared to tau-rich regions. These results could be consistent with the presence of a high-density, low-affinity binding site.

Marquié and colleagues (2015) have reported that flortaucipir binds with high affinity in areas that also are rich in neuromelanin, which could contribute to the apparent flortaucipir signal near what may be substantia nigra in the midbrain. A similar locus of flortaucipir retention has also been reported in another recent study (Johnson *et al.*, 2016). Also, the extent of age-related flortaucipir retention in the hippocampus region of interest, and particularly the region that appears to overlap choroid plexus, while consistent with other recently reported flortaucipir imaging studies (Jack *et al.*, 2016; Johnson *et al.*, 2016), was not anticipated at the outset of any of these studies. Although the neuropathology literature has suggested early tau accumulation (Braak stage 1–2) in ventral mesial temporal structures, the choroid plexus has not been a focus of previous investigation. However, a recent histopathologic study demonstrated the presence of AT8 immunoreactive phosphotau in the choroid plexus, suggesting the observed retention on PET imaging may be on-target binding to

aggregated tau in Biondi 'ring' tangles (Ikonomovic *et al.*, 2016) although this is not a consistent finding (Lowe *et al.*, 2016).

In summary, mesial temporal (amygdala and hippocampus/choroid plexus) flortaucipir retention increased with age regardless of amyloid status. In contrast, in Aβ+ subjects neocortical flortaucipir retention increased with diagnostic severity in a pattern reminiscent of the cross-sectional distribution of tau reported in post-mortem pathology studies (Braak and Braak, 1991, Braak *et al.*, 2006). These results are consistent with the hypothesis (Jack *et al.*, 2013) that tau and amyloid pathology may begin independently, and with the suggestion that spread of tau beyond mesial temporal lobe in Alzheimer's disease is associated with, and may be dependent on, amyloid accumulation. Elevated flortaucipir tau binding was associated with an increased prevalence of cognitive impairment, as assessed by MMSE and ADAS, especially in subjects under the age of 75, consistent with the hypothesis that cortical tau may be proximally associated with neuronal dysfunction and associated cognitive impairment in Alzheimer's disease. Together these results support further evaluation of flortaucipir tau PET imaging as a possible tool for aiding diagnosis, staging disease, and monitoring effects of Alzheimer's disease therapies.

Acknowledgements

The authors would like to acknowledge Brian F. Teske, Ph.D (Eli Lilly and Company) for assistance in manuscript preparation.

Funding

This study was sponsored by Avid Radiopharmaceuticals, a wholly owned subsidiary of Eli Lilly and Company.

Conflicts of interest

M.J.P, M.D.D.Sr, M.N., M.L., A.K.A., A.M., N.C.L., H.X., A.D.J., A.S., and M.A.M are employees of Avid Radiopharmaceuticals, a wholly owned subsidiary of Eli Lilly and Company. Florbetapir ^{18}F is an Eli Lilly product. S.S. receives research support and consultancy fees from Lilly, Biogen, Merck, Genentech, and Roche. He also receives research support from Avid, Novartis, and Functional Neuromodulation. D.J. is an employee of Molecular Neuroimaging, F.W.S does not have a conflict of interest to declare outside of this work.

Supplementary material

Supplementary material is available at *Brain* online.

References

Anand R, Gill KD, Mahdi AA. Therapeutics of Alzheimer's disease: past, present and future. Neuropharmacology 2014; 76 (Part A): 27–50.

Bolmont T, Clavaguera F, Meyer-Luehmann M, Herzig MC, Radde R, Staufenbiel M, et al. Induction of tau pathology by intracerebral infusion of amyloid-beta-containing brain extract and by amyloid-beta deposition in APP x tau transgenic mice. Am J Pathol 2007; 171: 2012–20.

Bouras C, Hof PR, Giannakopoulos Pl, Michel JP, Morrison JH. Regional distribution of neurofibrillary tangles and senile plaques in the cerebral cortex of elderly patients: a quantitative evaluation of a one-year autopsy population from a geriatric hospital. Cerebral Cortex 1994; 4: 138–50.

Braak H, Alafuzoff I, Arzberger T, Kretzschmar H, Del Tredici K. Staging of Alzheimer disease-associated neurofibrillary pathology using paraffin sections and immunocytochemistry. Acta Neuropathol 2006; 112: 389–404.

Braak H, Braak E. Neuropathological stageing of Alzheimer-related changes. Acta Neuropathol 1991; 82: 239–59.

Brier MR, Gordon B, Friedrichsen K, McCarthy J, Stern A, Christensen J et al. Tau and Aβ imaging, CSR measures, and cognition in Alzheimer's disease. Sci Transl Med 2016; 8: 338ra66.

Chhatwal JP, Schultz AP, Marshall GA, Boot B, Gomez-Isla T, Dumurgier J et al. Temporal T807 binding correlates with CSF tau and phospho-tau in normal elderly. Neurology 2016; 87: 920–6.

Chien DT, Szardenings AK, Bahri S, Walsh JC, Mu F, Xia C, et al. Early clinical PET imaging results with the novel PHF-Tau radioligand [F18]-T808. J Alzheimers Dis 2014; 38: 171–84.

Cho H, Choi JY, Hwang MS, Kim YJ, Lee HM, Lee HS et al. In vivo cortical spreading patter of tau and amyloid in the Alzheimer's disease spectrum. Ann Neurol. 2016a; 80: 247–58.

Cho H, Choi JY, Hwang MS, Lee JH, Kim YJ, Lyoo CH et al. Tau PET in Alzheimer disease and mild cognitive impairment. Neurology 2016b; 87: 375–83.

Clark CM, Pontecorvo MJ, Beach TG, Bedell BJ, Coleman RE, Doraiswamy PM, et al. Cerebral PET with florbetapir compared with neuropathology at autopsy for detection of neuritic amyloid-beta plaques: a prospective cohort study. Lancet Neurol 2012;11: 669–78.

Crary JF, Trojanowski JQ, Schneider JA, Abisambra JF, Abner EL, Alafuzoff I, et al. Primary age-related tauopathy (PART): a common pathology associated with human aging. Acta Neuropathol 2014; 128: 755–66.

Curtis C, Gamez JE, Singh U, Sadowsky CH, Villena T, Sabbagh MN, et al. Phase 3 trial of flutemetamol labeled with radioactive fluorine 18 imaging and neuritic plaque density. JAMA Neurology 2015; 72: 287–94.

Del Ser T, Steinwachs KC, Gertz HJ, Andres MV, Gomez-Carrillo B, Medina M, et al. Treatment of Alzheimer's disease with the GSK-3 inhibitor tideglusib: a pilot study. J Alzheimers Dis 2013; 33: 205–15.

Friston KJ, Ashburner JT, Kiebel SJ, Nichols TE, Penny WD, editors. Statistical parametric mapping: the analysis of functional brain images. London: Academic Press; 2007.

Fonov VS, Evans AC, McKinstry RC, Almli CR, Collins DL. Unbiased nonlinear average age-appropriate brain templates from birth to adulthood. NeuroImage 2009; 47: S102.

Giacobini E, Gold G. Alzheimer disease therapy[mdash]moving from amyloid-[beta] to tau. Nat Rev Neurol 2013; 9: 677–86.

Goedert M, Spillantini MG, Cairns NJ, Crowther RA. Tau proteins of alzheimer paired helical filaments: abnormal phosphorylation of all six brain isoforms. Neuron 1992; 8: 159–68.

Gordon BA, Friedrichsen K, Brier M, Blazey T, Su Y, Christensen J et al. The relationship between cerebrospinal fluid markers of Alzheimer pathology and positron emission tomography tau imaging. Brain 2016; 139 (Pt 8): 2249–60.

Hardy J, Selkoe DJ. The amyloid hypothesis of Alzheimer's disease: progress and problems on the road to therapeutics. Science 2002; 297: 353–56.

Holtzman DM, Carrillo MC, Hendrix JA, Bain LJ, Catafau AM, Gault LM, et al. Tau: from research to clinical development. Alzheimers Dement. 2016; 12: 1033–39.

Hyman BT, Phelps CH, Beach TG, Bigio EH, Cairns NJ, Carrillo MC, et al. National institute on aging Alzheimer's association guidelines for the neuropathologic assessment of Alzheimer's disease. Alzheimers Dement 2012; 8: 1–13.

Ikonomovic MD, Abrahamson EE, Price JC, Mathis CA, Klunk WE. [F-18]AV-1451 PET retention in choroid plexus: more than "off target" binding. Ann Neurol. 2016; 80: 307–8.

Jack CR, Knopman DS, Jagust WJ, Shaw LM, Aisen PS, Weiner MW, et al. Hypothetical model of dynamic biomarkers of the Alzheimer's pathological cascade. Lancet Neurol 2010; 9: 119–28.

Jack CR, Knopman DS, Jagust WJ, Petersen RC, Weiner MW, Aisen PS, et al. Tracking pathophysiological processes in Alzheimer's disease: an updated hypothetical model of dynamic biomarkers. Lancet Neurol 2013;12: 207–16.

Jack CR, Therneau TM, Wiste HJ, Weigand SD, Knopman DS, Lowe VJ, et al. Transition rates between amyloid and neurodegeneration biomarker states and to dementia: a population-based longitudinal cohort study. Lancet Neurol 2016; 15: 56–64.

Johnson KA, Schultz A, Betensky RA, Becker JA, Sepulcre J, Rentz D, et al. Tau positron emission tomographic imaging in aging and early Alzheimer disease. Ann Neurol 2016; 79: 110–19.

Joshi AD, Pontecorvo MJ, Lu M, Grundman M, Skovronsky DM, Mintun MA, et al. A semi-automated method for quantification of florbetapir F 18 PET images. J Nucl Med, 2015; 56: 1736–41.

Kidd M. Paired helical filaments in electron microscopy of Alzheimer's disease. Nature 1963; 197: 192–3.

Lewis J, Dickerson DW, Lin WL, Chisholm L, Corral A, Jones G, et al. Enhanced neurofibrillary degenereration in transgenic mice expressing mutant tau and APP. Science 2001; 293: 1487–91.

Lockhart SN, Baker SL, Okamura N, Furukawa K, Ishiki A, Furumoto S et al. Dynamic PET measures of tau accumulation in cognitively normal older adults and Alzheimer's disease patients measured using [18F] THK-5351. PLoS One 2016; 11: e0158460.

Lowe VJ, Curran G, Fang P, Liesinger AM, Josephs KA, Parisi JE et al. An autoradiographic evaluation of AV-1451 Tau PET in dementia. Acta Neuropathologica Communications 2016; 4: 58.

Marquié M, Normandin MD, Vanderburg CR, Costantino IM, Bien EA, Rycyna LG, et al. Validating novel tau positron emission tomography tracer [F-18]-AV-1451 (T807) on postmortem brain tissue. Ann Neurol 2015; 78: 787–800.

Maruyama M, Shimada H, Suhara T, Shinotoh H, Ji B, Maeda J, et al. Imaging of tau pathology in a tauopathy mouse model and in Alzheimer patients compared to normal controls. Neuron 2013; 79: 1094–108.

Masters CL, Simms G, Weinman NA, Multhaup G, McDonald BL, Beyreuther K. Amyloid plaque core protein in Alzheimer disease and down syndrome. Proc. Natl Acad Sci 1985; 82: 4245–9.

Middleton LE, Grinberg LT, Miller B, Kawas C, Yaffe K. Neuropathologic features associated with Alzheimer disease diagnosis: age matters. Neurology 2011;77: 1737–44.

Murray ME, Graff-Radford NR, Ross OA, Petersen RC, Duara R, Dickson DW. Neuropathologically defined subtypes of Alzheimer's disease with distinct clinical characteristics: a retrospective study. Lancet Neurol 2011; 10: 785–96.

Nelson PT, Jicha GA, Schmitt FA, Liu H, Davis DG, Mendiondo MS, et al. Clinicopathologic correlations in a large Alzheimer disease center autopsy cohort: neuritic plaques and neurofibrillary tangles "do count" when staging disease severity. J Neuropathol Exp Neurol 2007; 66: 1136–46.

Okamura N, Furumoto S, Harada R, Tago T, Yoshikawa T, Fodero-Tavoletti M, et al. Novel ^{18}F-labeled arylquinoline derivatives for noninvasive imaging of tau pathology in Alzheimers disease. J Nucl Med 2013; 54: 1420–27.

Okamura N, Furumoto S, Fodero-Tavoletti MT, Mulligan RS, Harada R, Yates P et al. Non-invasive assessment of Alzheimer's disease neurofibrillary pathology using 18F-THK5105 PET. Brain 2014; 137(Pt 6): 1762–71.

Ossenkoppele R, Schonhaut DR, Scholl M, Lockhart SN, Ayakta N, Baker SL et al. Tau PET patterns mirror clinical and neuroanatomical variability in Alzheimer's disease. Brain 2016; 139(Pt 5): 1551–67.

Pooler AM, Noble W, Hanger DP. A role for tau at the synapse in Alzheimer's isease pathogenisis. Neuropharmacology 2014; 76: 1–8.

Prohovnik I, Perl DP, Davis KL, Libow L, Lesser G, Haroutunian V. Dissociation of neuropathology from severity of dementia in late-onset Alzheimer disease. Neurology 2006;66: 49–55.

Querfurth HW, LaFerla FM. Alzheimer's disease. NEJM 2010; 362: 329–44.

Riley KP, Snowdon DA, Markesbery WR. Alzheimer's neurofibrillary pathology and the spectrum of cognitive function: findings from the Nun Study. Ann Neurol 2002; 51: 567–77.

Sabri O, Sabbagh MN, Seibyl J, Barthel H, Akatsu H, Ouchi Y, et al. Florbetaben PET imaging to detect amyloid beta plaques in Alzheimer's disease: phase 3 study. Alzheimers Dement 2015; 11: 964–74.

Sander K, Lashley T, Gami P, Gendron T, Lythgoe MF, Rohrer JD, et al. Characterization of tau positron emission tomography tracer [18F] AV-1451 binding to postmortem tissue in Alzheimer's disease, primary tauopathies, and other dementias. Alzheimers Dement 2016; 12: 1116–124.

Shcherbinin S, Schwarz AJ, Joshi A, Navitsky M, Flitter M, Shankle WR, et al. Kinetics of the tau PET tracer [^{18}F]-AV-1451 (T807) in subjects with normal cognitive function, mild cognitive impairment and Alzheimer's disease. J Nucl Med 2016; 57: 1535–42. jnumed.115.170027.

Schöll M, Lockhart SN, Schonhaut DR, O'Neil JP, Janabi M, Ossenkoppele R, et al. PET imaging of tau deposition in the aging human brain. Neuron 2016; 89: 971–82.

Schwarz AJ, Yu P, Miller BB, Shcherbinin S, Dickson J, Navitsky M, et al. Regional profiles of [^{18}F]-AV-1451 tau PET images recapitulate key features of Braak histopathological stages. Brain 2016; 139 (Pt 5): 1539–50.

Selkoe DJ. The molecular pathology of Alzheimer's disease. Neuron 1991; 6: 487–98.

Sperling RA, Aisen PS, Beckett LA, Bennett DA, Craft S, Fagan AM, et al. Toward defining the preclinical stages of Alzheimer's disease: recommendations from the National Institute on Aging-Alzheimer's Association workgroups on diagnostic guidelines for Alzheimer's disease. Alzheimers Dement 2011; 7: 280–92.

Stancu IC, Vasconcelos B, Terwel D, Dewachter I. Models of β-amyloid induced tau-pathology: the long and folded road to understand the mechanism. Mol Neuroidegen 2014; 9: 51–64.

Tomlinson BE, Blessed G, Roth M. Observations on the brains of demented old people. J Neurol Sci 1970; 11: 205–42.

Vasconcelos B, Stancu IC, Buist A, Bird M, Wang P, Vanoosthuyse A, et al. Heterotypic seeding of tau fibrillization by pre-aggregated Abeta provides potent seeds for prion-like seeding and propagation of Tau-pathology in vivo. Acta Neuropathol. 2016; 131: 549–569.

Xia CF, Arteaga J, Chen G, Gangadharmath U, Gomez LF, Kasi D, et al. [18F]T807, a novel tau positron emission tomography imaging agent for Alzheimer's disease. Alzheimers Dement 2013; 9: 666–76.

Yanamandra K, Kfoury N, Jiang H, Mahan TE, Ma S, Maloney SE, et al. Anti-tau antibodies that block tau aggregate seeding in vitro markedly decrease pathology and improve cognition in vivo. Neuron 2013; 80: 402–14.